Original Research Paper

Development and tableting of directly compressible powder from electrospun nanofibrous amorphous solid dispersion

B. Démuth [a], A. Farkas [a], B. Szabó [a], A. Balogh [a], B. Nagy [b], E. Vágó [c], T. Vigh [d], A.P. Tinke [e], Z. Kazsu [f], Á. Demeter [f], J. Bertels [d], J. Mensch [d], A. Van Dijck [d], G. Verreck [d], I. Van Assche [d], G. Marosi [a,*], Z.K. Nagy [a,*]

[a] Department of Organic Chemistry and Technology, Budapest University of Technology and Economics (BME), 1111 Budapest, Műegyetem rkp. 3, Hungary
[b] Quick2000 Ltd., 4400 Tiszavasvári, Kabay J.u. 29, Hungary
[c] Department of Chemical and Environmental Process Engineering, Budapest University of Technology and Economics (BME), 1111 Budapest, Műegyetem rkp. 3, Hungary
[d] Drug Product Development, Janssen R&D, 2340 Beerse, Turnhoutseweg 30, Belgium
[e] Department of API Small Molecule Development, Chemical Technology and Process Control, Janssen R&D, 2340 Beerse, Turnhoutseweg 30, Belgium
[f] Drug Polymorphism Research, Gedeon Richter Plc, Gyömrői út 30-32, H-1103 Budapest, Hungary

ARTICLE INFO

ABSTRACT

This work was carried out to explore the unknown area of converting non-woven fibres, prepared by high speed electrospinning, into a directly compressible blend by mixing with excipients. An experimental design, with independent variables of compression force and fillers fraction, was realized to investigate tabletability of electrospun material (EM) and to produce hard tablets with appropriate disintegration time. The models proved to be adequate; fitted to the results and predicted values well for the optimal tablet, which was found to be at 76.25% fillers fraction and 6 kN compression force. Besides standard characterizations, distribution of EM was investigated by Raman mapping and scanning electron microscopy revealing the propensity of EM to cover the surface of microcrystalline cellulose and not of mannitol. These analytical tools were also found to be useful at investigating the possible formation of the so-called gelling polymer network in tablets. Scanning electron microscopic pictures of tablets confirmed the maintenance of fibrous structure after compression. The moisture absorption of EM under increasing humidity was studied by dynamic vapour sorption measurement, which suggested good physical stability at 25 °C and 60% relative humidity (corroborated by modulated DSC). These results demonstrate the feasibility of a pharmaceutically acceptable downstream processing for EMs.

1. Introduction

The challenge to make drug candidates of poor water solubility suitable for commercialisation has been investigated for decades. Several new ideas and technologies have been introduced in order to enhance the bioavailability of such active pharmaceutical ingredients (APIs). One of the most promising methods is the formation of amorphous solid dispersions (ASDs) [1–3] owing to the advantageous dissolution characteristics of the amorphous form of a drug. To prepare these dispersions melt extrusion and spray drying have emerged as the most important technologies and they are still vividly investigated [4–8]. There are already several products on the market containing ASD prepared by melt extrusion or spray drying [2]. This also means that their downstream processing techniques are developed [9] although in most cases many unique issues can emerge during downstream of the solid dispersion, which therefore needs to be investigated separately. For instance, it might be challenging to mill a melt extrudate [10] or sometimes the inherent poor compressibility of glassy or rubbery extrudates requires a lot of fillers during compression [11,12]. In case of spray dried dispersion the very low bulk density and the poor flowability (due to the small particle size) often pose challenge to experts of formulation [4,13]. A strategy has been developed recently to control and lower residual solvent content in spray-dried solid dispersion [14], which is of great importance of solvent technologies.

Tablets have obvious advantages over other formulations whereby they add up to 80% of all formulations. Thus, formulation of tablets is generally the first goal of a pharmaceutical company with a new API (considering the patient compliance, convenient storage, good mechanical properties and precise dosing) even if it

* Corresponding author.
  E-mail addresses: gmarosi@mail.bme.hu (G. Marosi), zsknagy@oct.bme.hu (Z.K. Nagy).

might be very challenging (e.g. creation of free flowing powder, good compressibility). In case of ASD there is one extra, serious challenge: the maintenance of the physical stability of the amorphous API during the whole downstream processing and storage [9,15]. Granulation (especially wet granulation due to presence of water) can induce phase separation and recrystallization [16,17] of the API; therefore, direct compression is always the preferred route. However, phase separation upon compression has been also published [18,19]. Although the direct compression of ASDs might be very complex it was chosen in the present work for forming tablets from fibrous ASD.

Electrostatic spinning is a promising technology in the pharmaceutical industry for the production of ASDs for oral drug delivery [20–28] or other applications [29–31]. Just like the aforementioned two techniques (spray drying and melt extrusion), this is also a continuous technology [32,33]. Electrospinning, for pharmaceutical purposes, has been investigating since 2003 (wound healing and drug loaded nanofibres) [34,35]. Promising results in pharma industry compatible scaling-up of electrospinning have been achieved by creating high speed electrospinning [22,26]. However, the downstream process has still never been investigated thoroughly. According to the author's best knowledge, this is the first paper discussing a trial to convert an electrospun nanofibrous mat into a directly compressible powder to prepare tablets. The investigation of dynamic vapour sorption of EM (and the related modulated differential scanning calorimetry studies) was included as well as an experimental design to optimize disintegration time and tensile strength of tablets. Design of experiments approach is often applied to optimize pharmaceutical powders [36]. Furthermore, unique peculiarities of EM have been determined in blends and tablets with scanning electron microscopy and Raman mapping.

2. Materials and methods

2.1. Materials

Itraconazole (ITR), vinylpyrrolidone-vinyl acetate 6:4 copolymer (PVPVA64) and magnesium stearate were provided by Janssen Pharmaceutica (Beerse, Belgium). Aerosil® 200 was purchased from Evonik Industries (Essen, Germany). Microcrystalline cellulose (Vivapur® 200, MCC) was given by JRS Pharma (Rosenberg, Germany). Lactose (Tablettose® 80) was received from Meggle Pharma (Wasserburg, Germany). Mannitol (Pearlitol® 400DC) was a kind gift from Roquette Pharma (Lestrem, France). Kollidon® CL was supplied by BASF (Ludwigshafen, Germany).

2.2. Preparation of electrospun material (EM) by high speed electrospinning

The EM was prepared according to the description provided by Nagy et al. [26]. The high speed electrospinning of the solution of PVPVA64 (60%) and ITR (40%) in dichloromethane-ethanol (ratio is 2:1; 225 mg PVPVA64 and 150 mg ITR in 1 ml solvent mixture) was performed under the following conditions: 50 kV voltage, 40,000 rpm spinneret rotational speed, 1500 mL/h feeding rate, ambient temperature. Further information and the basic characterization can be found in the aforementioned article. Prior to further application the obtained sheet was passed through a sieve with 0.95 mm holes to make it suitable for blending.

2.3. Dynamic vapour sorption (DVS)

The DVS measurement was performed on a DVS Intrinsic instrument (Surface Measurement Systems, London, UK). The relative humidity (RH) was altered every hour by 10% from 0 up to 95%. The measurement was carried out on two different temperatures: 25 °C and 40 °C. Two sorption and desorption cycles were collected. The weight of the sample was measured continuously on a SMS UltraBalance™.

2.4. Modulated differential scanning calorimetry (mDSC)

The EM was analysed in a DSC Q2000 instrument (TA Instruments, Crawley, UK) by "Heat only" modulation mode, with a heating rate of 2 °C/min, an amplitude of 0.318 °C and a period of 60 s. Standard aluminium pans (TA instruments) were applied with crimping. Samples were kept in climate chambers at 25 °C/60% RH or 40 °C/75% RH in open holders for the stability test.

2.5. Experimental design for preparation of fast disintegrating tablets

Firstly, a 2^2 design was planned in order to study the compression behaviour of the EM. The compression force and the fillers fraction were selected as independent variables. The fraction of the fillers was calculated from the weight of the fillers and EM to highlight their ratio since it might have a significant effect on the formation of a gelling polymer network [9]. Levels of independent variables were selected based on preliminary experiments to achieve an appropriate range for dependent variables (disintegration time and tensile strength). Centrum point measurements were added to the design to check the adequacy. However, the fitted linear model was not adequate; hence the design was expanded to a 3^2 randomized full factorial design where quadratic effects can be introduced. Composition of tableting blends can be observed in Table 1, while levels of independent variables in Table 2. Tensile strength and disintegration time were chosen as dependent variables since these values can be measured rather precisely and independent variables might have a significant effect on them. Tensile strength was calculated from hardness as the following [37]:

$$T = \frac{2 \cdot H}{\pi \cdot t \cdot d}$$

where T is the tensile strength, H is hardness, t is thickness of the tablets, while d is the diameter of the punches and tablets (9.5 mm).

Three tablets were measured in each case (to obtain standard deviation and increase the reliability of the design) and individual results were evaluated with Statistica 12 (Tulsa, Oklahoma, USA). Every measurement was performed by one person to minimalize the error. Our purpose was to optimize the compression force and the composition for both dependent variables (low disintegration time, high tensile strength). Furthermore, it was intended to maintain the structure of the fibres in tablets as good dissolution properties can be attributed to this.

2.6. Preparation of blends

All excipients were pushed through a sieve with 0.95 mm holes prior to blending. Mixing was carried out with a Turbula® T2F shaker-mixer (Glenn Mills Inc., Clifton, NJ, USA) for 5 min (magnesium stearate was mixed separately after other excipients).

2.7. Characterization of blends

A granulometry study was carried out for two blends (presumably centre blend has intermediate characteristics). Bulk and tapped densities were determined with 100 g of the blends. Tapped density was measured after 1250 taps on an ERWEKA SVM 12 tapping volumeter (Heusenstamm, Germany). Also 100 g was applied for the sieve analysis. The used sieves: 1000 μm,

Table 1
The characterization of the terminal blends.

	Material	Blend 1	Centre blend	Blend 2
Composition	EM (mg)	125 (25%)	125 (22.4%)	125 (19.5%)
	MCC (mg)	157 (31.5%)	183 (32.8%)	219 (34.2%)
	Mannitol (mg)	157 (31.5%)	183 (32.8%)	219 (34.2%)
	Kollidon CL (mg)	50 (10%)	56 (10%)	65 (10%)
	Aerosil 200 (mg)	5 (1%)	5.6 (1%)	6.5 (1%)
	Mg-stearate (mg)	5 (1%)	5.6 (1%)	6.5 (1%)
	Flowability index			
Flowability	Bulk density	0.405 g/cm³	–	0.437 g/cm³
	Tapped density	0.535 g/cm³	–	0.592 g/cm³
	Hausner ratio	1.32	–	1.35
	Carr index	24.3	–	26.2
	Angle of repose[a]	58.13°	–	55.20°
	True density	1.4079 g/cm³	–	1.4003 g/cm³
	Sieve size	Blend 1	Blend 2	EM
Particle size distribution	Pan	31.8%	27.5%	22.6%
	38 µm	–	28.0%	
	75 µm	12.9%	12.5%	8.10%
	150 µm	14.8%	15.0%	39.4%
	250 µm	36.8%	39.8%	1.45%
	500 µm	3.30%	4.97%	0.40%
	850 µm	0.25%	0.13%	0.05%
	1000 µm	0.15%	0.10%	–

[a] The used method is described in Section 2.7.

Table 2
The factors of the performed experimental design and the obtained results.

Batch number	Compression force (kN)	Fillers fraction (%)*	Tensile strength (N/mm²)	Disintegration time (s)	Friability (%)
F1	3.0	71.4	0.67 ± 0.08	98 ± 9	1.09
F2	4.5	71.4	1.37 ± 0.10	289 ± 80	–
F3	6.0	71.4	2.23 ± 0.03	832 ± 56	0.08
F4	3.0	74.6	0.60 ± 0.01	38 ± 4	–
F5	4.5	74.6	1.20 ± 0.05	226 ± 24	0.34
F6	6.0	74.6	1.96 ± 0.12	343 ± 105	–
F7	3.0	77.8	0.52 ± 0.02	25 ± 4	1.01
F8	4.5	77.8	1.03 ± 0.03	93 ± 12	–
F9	6.0	77.8	1.84 ± 0.09	363 ± 15	0.02
Optimized tablets (OT)	6.0	76.25	1.94 ± 0.04	337 ± 36	–

$\left(\frac{m_{fillers}}{m_{fillers}+m_{EM}}\right) \cdot 100.$

850 µm, 500 µm, 250 µm, 150 µm, 75 µm (in case of the pure EM a 38 µm sieve instead of the 1000 µm sieve in order to assess the distribution better at low particle sizes). Shaking was executed on a Retsch® sieve shaker (Haan, Germany) with applying 1.5 mm amplitude for 5 min. Angle of repose was measured on an in-house built flow meter containing a platform (with fixed diameter) and a cylinder (with the same outer diameter like the platform). Powder is poured into the cylinder where it touches the platform and it starts to flow off of the flat platform due to the upward movement of the cylinder (speed was fixed) while forming a pile. Angle of repose can be determined based on the position of the cylinder which has to be moved to the top of the pile after the falling of the powder stopped. This method generally provides larger angle values but with lower deviations compared to the widely used angle of repose determination. True densities of the blends were determined on an Accupyc 1330 helium pycnometer (Micromeritics, Atlanta, GA, USA).

2.8. Scanning electron microscope (SEM)

SEM images of the blends were taken with a Phenom Pro instrument (PhenomWorld, Eindhoven, The Netherlands). Each specimen was fixed by conductive double-sided carbon adhesive tape and coated by gold prior SEM imaging. 10 kV was applied as accelerating voltage and scanning was conducted with secondary electron detection.

Broken surfaces of tablets were investigated by a JEOL 6380LVa (JEOL, Tokyo, Japan) type scanning electron microscope. Tablets were fixed by a conductive double-sided carbon adhesive tape and coated by gold prior SEM imaging. The applied accelerating voltage was 15 kV.

2.9. Preparation of tablets

Tablets were compressed on a Huxley Bertram hydraulic compaction simulator equipped with 9.5 mm flat-face punches and instrumented die. The compression profiles were created with the compaction simulator software for a Courtoy Modul S press (B-tooling). A 1 s profile was applied and pre-compression load was held at 50% of the main compression load.

2.10. Characterization of tablets

Hardness was measured on an ERWEKA TBH30 hardness tester with three tablets. Disintegration time was determined on an ERWEKA ZT71 disintegration tester in tap water at 37 °C with three tablets. Friability was measured on ERWEKA TAR20 friability tester after 100 rounds on ten tablets.

2.11. Raman mapping of tablets

A Horiba Jobin-Yvon LabRAM system coupled with external 785 nm diode laser source and Olympus BX-40 optical microscope was used for collecting Raman mapping spectra. An objective of $10\times$ magnification (laser spot size: $\sim$4 μm) was applied in focusing and spectrum acquisition. The confocal hole of 500 μm, the half of maximum diameter, was employed in confocal system to improve the confocal performance decreasing the analysis volume. Finally, 950 groove/mm grating monochromator disperses the Raman photons before those reach the CCD detector. The spectrograph position was set to provide the spectral range of 460–1680 cm^{-1} and 3 cm^{-1} resolution. Tablets with two different API contents (one with optimized composition and one with very low (50%) filler fraction) were mapped by Raman instrument. The tablets were broken in two parts and Raman mapping was performed on the broken surface of the tablets. The maps were collected with 15 μm step size and consisted of 41 × 41 points. Every single spectrum was measured with acquisition time of 60 s and 2 spectra were averaged at each measured point.

2.12. In vitro dissolution test

The dissolution tests were carried out on a Pharmatest PTWS 600 dissolution tester (Pharma Test Apparatebau AG, Hainburg, Germany). Measurement parameters for neat EM: 900 mL 0.1 N HCl, modified USPII apparatus ("tapped basket" method [26]), 50 rpm paddle speed, room temperature. Measurement parameters for tablets: 900 mL 0.1 N HCl, USPII apparatus, 100 rpm paddle speed, room temperature. An on-line coupled Agilent 8453 UV–Vis spectrophotometer (Hewlett-Packard, Palo Alto, USA) was applied to measure the concentration of dissolved ITR at a wavelength of 254 nm. Each sample contained 50 mg of ITR.

3. Results and discussion

3.1. Characterization of EM with dynamic vapour sorption (DVS)

Stability of ASDs can be directly influenced by water uptake during downstream processing and storage. The T_g of ASD is lowered when water, acting as a plasticizer, is adsorbed. Below the T_g the mobility of the matrix polymer can allow the molecules of the API to move by diffusion and crystallize. DVS shows the water uptake (weight gain) under certain humidity values, and thus the stability of the EM can be predicted. According to the DVS sorption isotherms (Fig. 1) no crystallization of ITR occurred either at 25 °C or at 40 °C. If crystallization had taken place in course of DVS a remarkable decrease in water uptake could have been noticed after a certain humidity as crystalline materials, being less hygroscopic than the corresponding amorphous ones, adsorb significantly less water [38]. Presumably, at 40 °C (Fig. 1b) the molecular mobility is higher and water can penetrate into the bulk of the powder more easily and there is no difference between the two sorption cycles. However, at 25 °C (Fig. 1a) there is a hysteresis between the two sorption cycles with the second one looking more similar to the sorption cycles at 40 °C. Consequently, the first sorption cycle made the EM more susceptible for water uptake.

The DVS sorption isotherms can be divided into two linear sections and the part between them. During the first period moisture is predominantly adsorbed on the surface (first linear section, 10–50% RH), whilst from 70% RH the moisture begins to penetrate into the bulk of the material that starts to liquefy (second linear section, 80–95%). The transition point (intersection of the prolongation of the two linear sections), which gives the "glass transition relative humidity" [38], was found to be 72% at this ramping rate at both temperatures. Below that transition phase separation is not expected while above that it can occur.

3.2. Modulated differential scanning calorimetry (mDSC) investigations with EM

In order to detect phase separation or slight crystallization that might have occurred as a consequence of DVS treatment the samples were analysed by modulated DSC before and right after the DVS measurement. The initial sample possessed single glass transition temperature (T_g) around 90 °C (Fig. 2) meaning that the polymer and API were well-mixed (solid solution). The recorded temperature is in good correlation with the Fox-equation:

$$\frac{1}{T_g} = \frac{w_1}{T_{g,1}} + \frac{w_2}{T_{g,2}}$$

where T_g is the glass transition temperature of mixture, $T_{g,1}$ and $T_{g,2}$ are the glass transition temperatures of the components (in K) and w_1 and w_2 are the mass fractions of the components. The T_g of ITR and PVPVA64 are 59.4 °C [39] and 111.9 °C (latter is based on our own measurement), respectively [40]. The sample after DVS pretreatment at 25 °C exhibited multiple glass transitions at 62, 81 and 108 °C (Fig. 2), which belong to the API-rich, mixed and the polymer-rich phase, respectively [40]. Since no melting peak was observed ITR did not recrystallize at 25 °C, and thus it remained amorphous. According to these results even if phases become separated ITR is not prone to recrystallize at the 25 °C. However, the DVS pre-treatment at 40 °C proved to be intensive enough to generate recrystallization. The melting peak was not obviously apparent,
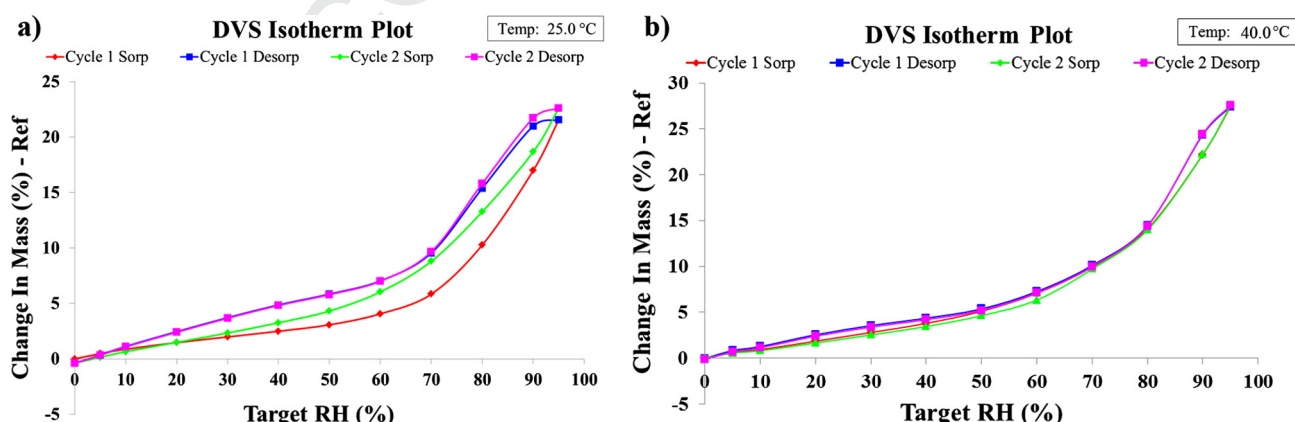

Fig. 1. The DVS diagram of EM at (a) 25 °C and (b) 40 °C.
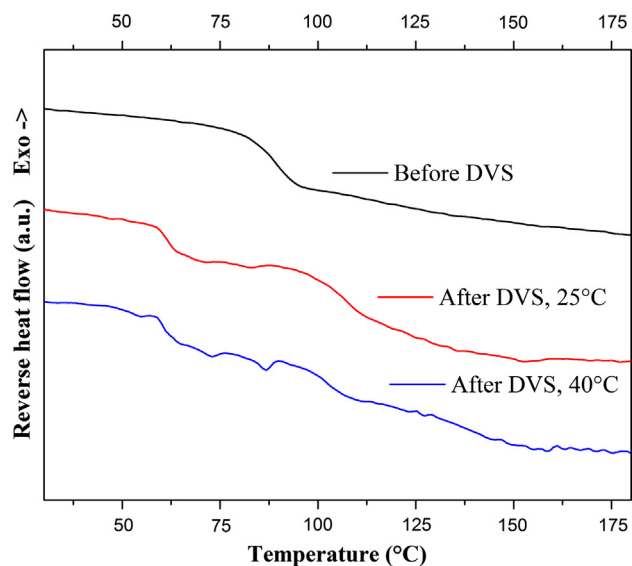
Fig. 2. Modulated DSC thermogram of EM before and after DVS.

but two new endothermic peaks appeared on the DSC thermogram (in the reverse heat flow) at 73 and 86 °C, which can be associated with the formation of the nematic phase of ITR [41].

Based on the results from DVS measurements (calculation of "glass transition humidity" and the difference between 25 and 40 °C) the fibrous ASD was supposed to be stable at 25 °C/60% RH (with no phase separation), but not at 40 °C/75% RH (with crystallization). This assumption was confirmed by a short-term stability test with mDSC (Fig. 3).

EM was placed in climate chambers for the stability test and removed directly before the mDSC measurements. The detected glass transition temperatures for the material after production and storage at 25 °C/60% RH after 1 day, 1 week and 1 month were 91.2 °C, 90.6 °C, 91.4 °C and 91.4 °C, respectively (Fig. 3a). The glass transition temperature did not decrease with time and no new glass transitions (or melting peak) have appeared on the thermogram, which confirms the unchanged status of the well-mixed components. However, at 40 °C/75% RH the peaks at 73 and 86 °C appeared after one day indicating the phase transition from amorphous to crystalline state. After one week, the sample clearly had a melting peak at 157 °C (Fig. 3b). In our previous work it was found that ITR in this nanofibrous ASD did not crystallize during a 1-year

stability test at 25 °C/60% RH in closed holder [22]. Presumably, no phase separation would occur during longer period.

3.3. Characterization of blends

The EM and each excipient were pushed through on a 0.95 mm sieve prior to further application. The composition of the tableting blends and the results of the granulometry study can be seen in Table 1.

Bulk, tapped and true densities and the angle of reposes of the blends are presented, furthermore Hausner ratios and Carr indexes were derived (Table 1). The two blends exhibited similar flow properties according to Hausner ratios, Carr index and angle of reposes. Compared to literature data, these values suggest fair to poor flowability for these blends although it does not seem impossible to carry out the downstream process with them.

No abnormality was found in the particle size distribution of the two blends, they possessed very similar distribution (Table 1).

According to SEM pictures of the sieve fractions, a significant part of the material in the pan is the EM (Fig. 4a) though EM can be found at larger particle size (75–500 μm) in aggregates (Fig. 4b) and on the surface of fillers, rather on MCC (Fig. 4c) than mannitol (Fig. 4d). MCC possesses a quite structured, while mannitol has a very flat surface; hence EM can more easily adhere to MCC.

The sieved EM (Fig. 5a) has in fact a diverse propensity to adhere to the surface of different fillers. Lactose served as a comparison since its surface is similarly structured like MCC and it is a sugar derivative like mannitol. More fibres can be found on MCC (Fig. 5b) and lactose (Fig. 5d) particles than on mannitol particles (Fig. 5c), which are "fibreless" on certain areas. This phenomenon might have significant effect on flowability, disintegration and dissolution.

3.4. Experimental design for the tableting of EM

In order to systematically study the effects of the compression force and fillers fraction on the disintegration time and tensile strength, a 3^2 full factorial design was planned. Friability was also measured for those tablets of the original 2^2 design to obtain information about it but evaluation for friability was not included in our purposes.

The design of experiments and the results can be seen in Table 2. The obtained hardness values were ranging from 70 N to 220 N.

The obtained values for every measured attribute belonged to the usual pharmaceutical ranges.
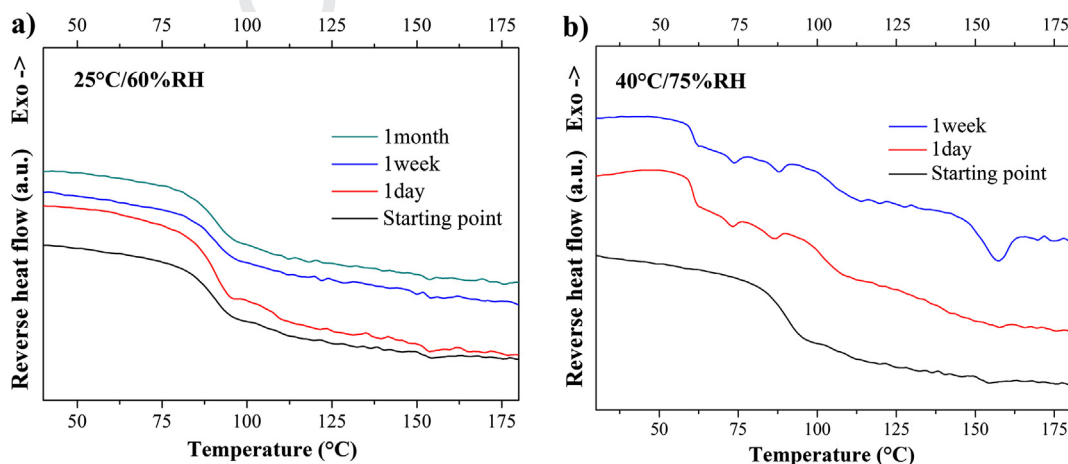

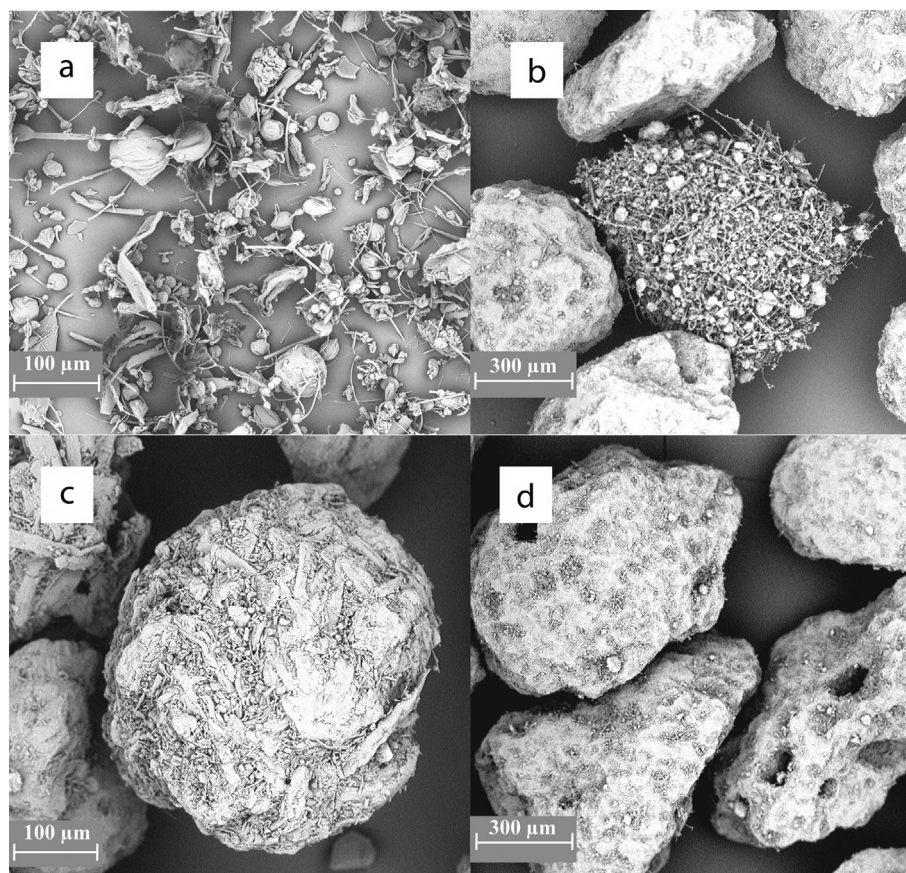**Fig. 3.** The short-term stability test of the EM at (a) 25 °C/60% RH and (b) 40 °C/75% RH (open conditions).

Fig. 4. SEM images of sieve fractions: (a) pan, (b) 500 μm, (c) 250 μm (MCC particle) and (d) 500 μm (mannitol particles).

3.4.1. The evaluation of the experimental design

For both dependent variables compression forces had the largest impact according to Pareto charts (data not shown), but other effects – including quadratic effects - were also found to be significant. However, for tensile strength these other effects can be considered negligible due to the large difference in significance compared to the linear effect of compression force. Therefore, a linear model between compression force and tensile strength is a relatively good approximation. This observation was confirmed on the fitted surface diagram (Fig. 6a) on which the tensile strength was depicted in function of the fillers fraction and compression force (according to the developed model). Tensile strength was changing with compression force in proportion but it did not change much with the increasing amount of fillers.

The obtained tablets had a disintegration time in the 0–14 min range which is acceptable in the pharmaceutical technology (immediate release tablets should disintegrate within 15 min). Since the variance was increasing with disintegration time the evaluation was carried out for the common logarithms of the data. Compression force had the largest impact on disintegration time, but - unlike in case of tensile strength - some of the other effects also seem to be of importance e.g. the linear effect of the fillers fraction possessed larger significance than for tensile strength. In this case linear model would not be adequate which can be confirmed by the fitted surface diagram (Fig. 6b).

There was an interesting saddle point around 76% fillers fraction and 6 kN compression force. At this point the disintegration time should be higher than at 77.8% fillers fraction as the fillers act as spacers among the EM particles facilitating the disintegration by hindering the formation of gelling polymer network. However, probably at this saddle point EM is dispersed in the tablet completely while fillers cannot disrupt more EM aggregates. With more MCC in the tablet, the bonding capacity is increased, hence the tablet is less prone to disintegrate. This phenomenon is also slightly visible on the tensile strength surface diagram though it is not as extensive as in case of disintegration time.

3.5. The optimization of the tablets

With the desirability function of Statistica software it was possible to determine an optimal composition and compression force in order to minimize the disintegration time and maximize tensile strength (both had the same coefficient). 76.25% fillers fraction and 6 kN compression force were found to be the optimum. 6 kN compression force is needed to achieve an appropriate tensile strength which is strongly correlated with friability. After the optimization, tablets with optimal settings were produced confirming the adequacy of our model. The predicted tensile strength and disintegration time were 1.88 N/mm^2 and 306 s, while experimental results were the following: 1.94 ± 0.04 N/mm^2 and 337 ± 36 s. With regards to the deviations of the experimental results the model can be considered precise and reliable predicting the values for dependent variables well. Furthermore, it anticipated that tablets with the optimal composition would have lower disintegration time than tablets with larger amount of filler at 6 kN compression load, which was found true. A design space, which seems to be of great importance when exploring this unknown area, can be defined by using design of experiments approach. Defining a design space is a cornerstone of the important and innovative pharmaceutical trend, Quality by Design (QbD) [42,43]. QbD has been recently applied also to optimize a spray drying process to obtain better ASDs from several views [44].
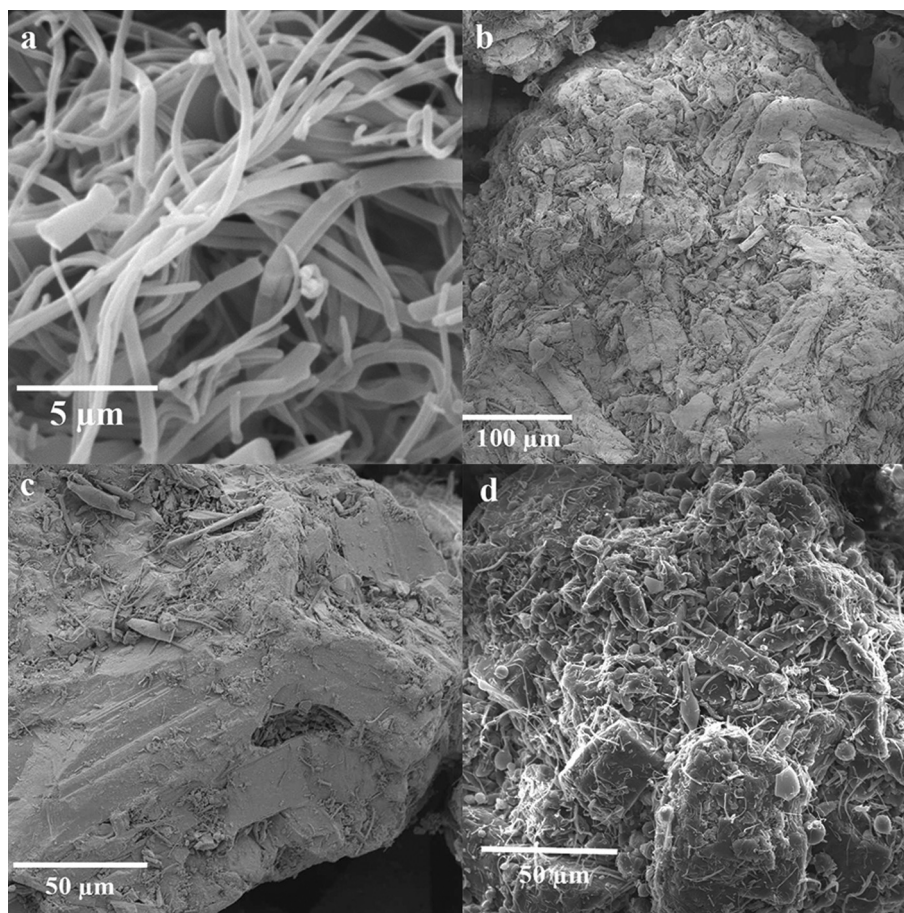
Fig. 5. SEM images of the (a) sieved EM, (b) EM-MCC, (c) EM-mannitol and (d) EM-lactose complexes.
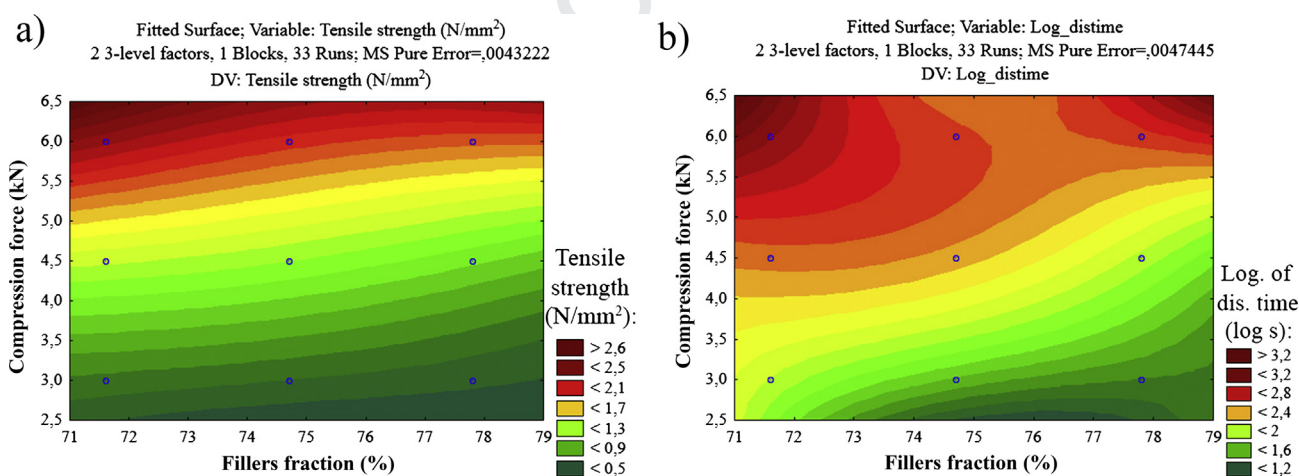

Fig. 6. The fitted surface diagram of (a) tensile strength and (b) disintegration time.

3.6. Investigation of gelling polymer network

The increase of disintegration time was steeper at low fraction of fillers than at high fraction, which indicates propensity of the polymer to form a gelling network. In order to investigate this phenomenon and distribution of EM, Raman mapping was carried out on the cross sections of two tablets: at fraction of 76.25% fillers and at fraction of 50% fillers (Fig. 7).

In Fig. 7 mannitol appears in large uniform areas (Fig. 7c) while mixed zones with EM and MCC can be observed as well (Fig. 7a and b). Interestingly, EM seems to occupy more space than it is supposed to do according to its amount in the tablet (Fig. 7a). This can be attributed to its low density and tendency to cover MCC with a layer resulting in apparent low value of local concentration of MCC. This is in accordance with SEM images showing the sieve fractions of tableting blend (Fig. 4).
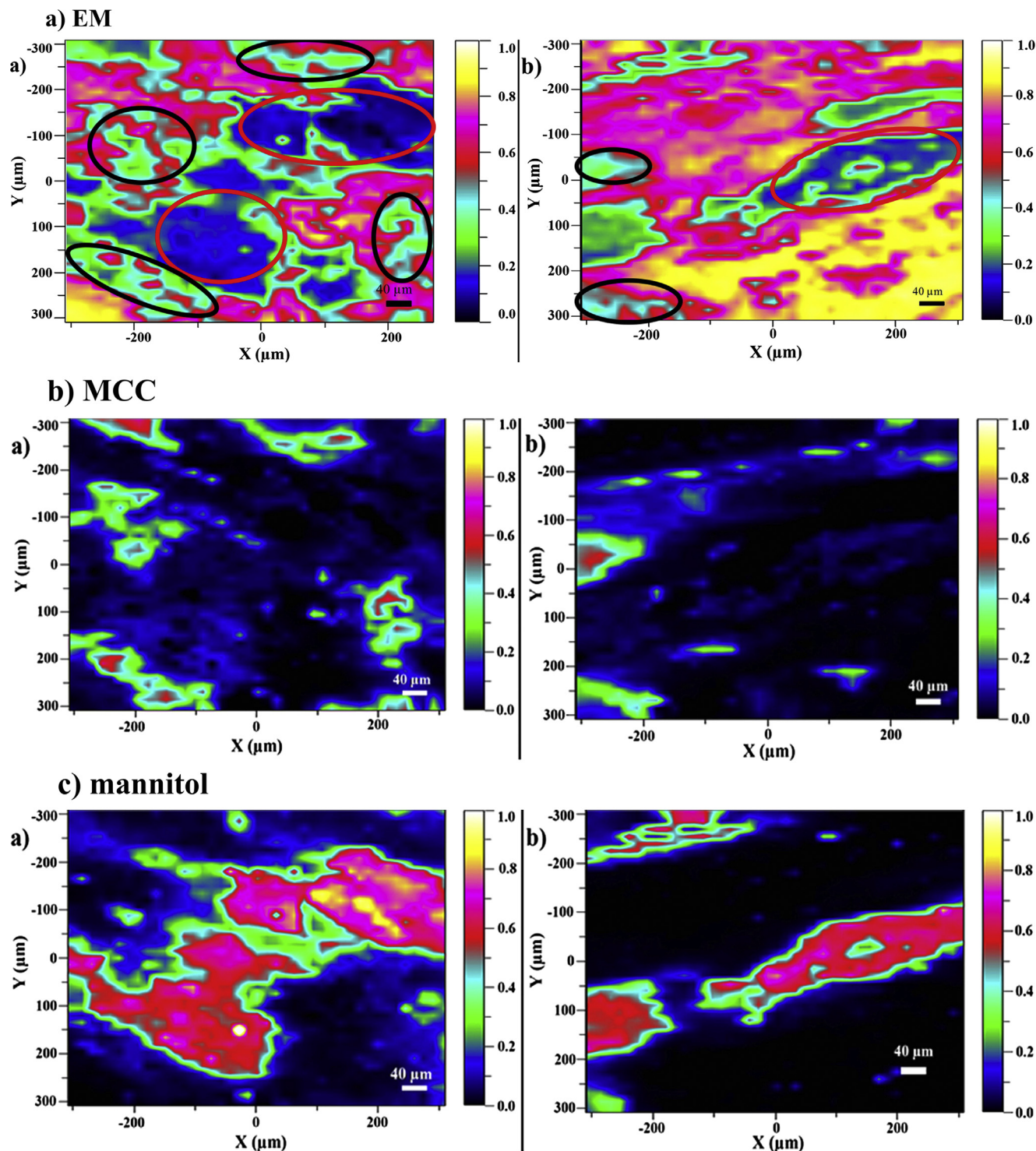
8   *B. Démuth et al./Advanced Powder Technology xxx (2017) xxx–xxx*

Fig. 7. Raman maps of tablets showing the spatial distribution of (a) EM, (b) MCC, (c) mannitol. Tablet showed on the left side comprised a fillers fraction of 76.25%, while the right one contained 50%. On the first two maps red circles indicates the sites of mannitol, black circles indicates the sites of MCC particles. (For interpretation of the references to colour in this figure legend, the reader is referred to the web version of this article.)

While the first tablet (on left side of Fig. 7) is a fast disintegrating tablet (disintegration time ~5 min) the second one (on right side of Fig. 7) does not disintegrate completely during 2 h (although in both cases 10% of disintegrant was incorporated in the tablet). Obviously, at higher EM ratio the EM particles are very close to each other whereby they can form a gelling polymer network that hinders the disintegration and thus the dissolution. This gelling polymer network is somewhat disrupted by large mannitol particles (for instance in the middle of the map) while it can continue on the MCC particles if it has a high concentration there.

The formation of gelling polymer network can also be studied on SEM images (Fig. 8a and b). The pictures were taken of the same tablets as the Raman maps. On the image of the tablet with less EM (Fig. 8a) a lot of separated areas can be discovered where fillers increase the distance among EM particles hindering the formation of gelling polymer network. On the other hand, the network of the
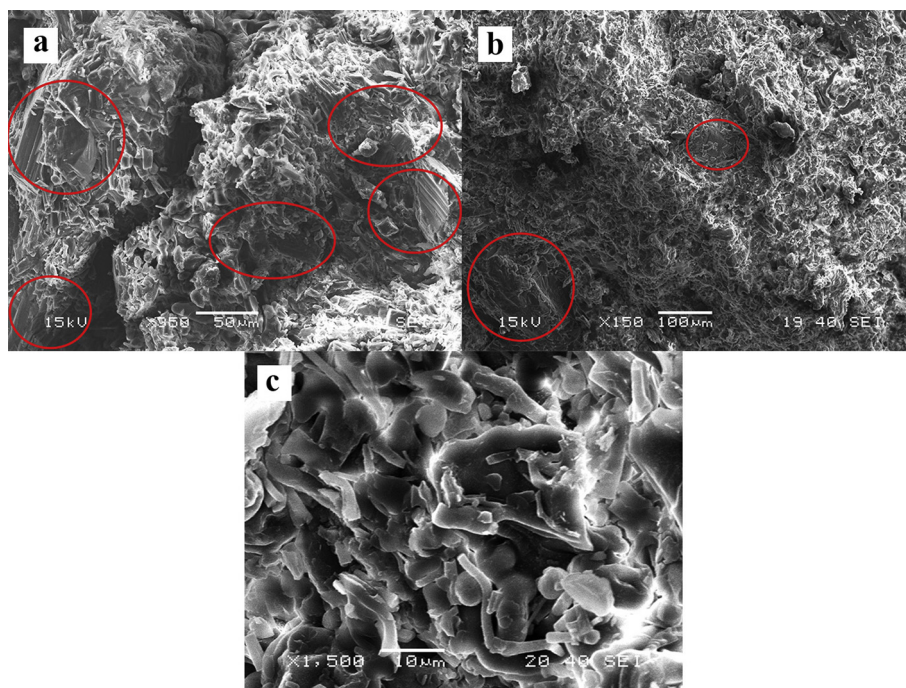
Fig. 8. SEM images of broken tablet surfaces (a) fillers fraction of 76.25%, (b) fillers fraction of 50%, (c) higher magnification to demonstrate the fibrous structure of EM in tablets (tablet with less fillers). Red circles indicate the discontinuities of the polymer network. (For interpretation of the references to colour in this figure legend, the reader is referred to the web version of this article.)
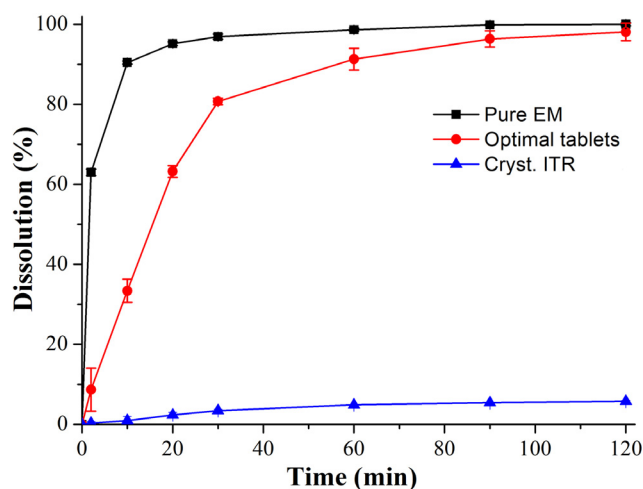

Fig. 9. Dissolution of ITR from pure EM, optimal tablets and crystalline ITR (n = 3).

EM is not disrupted with lower filler concentration as it is visible on the image of that tablet (Fig. 8b).

The preserved fibrous structure of EM in the tablets can be seen at larger magnification (Fig. 8c), which is the main reason why advantageous dissolution properties can be maintained in tablets (Fig. 9). It can be observed that supersaturated state and complete dissolution of ITR was achieved from tablets (just like from neat fibres) with low deviation of the dissolved amount.

4. Conclusions

This work presents the conversion of a fibrous electrospun material (EM) to tablet and the related characterizations, which meets urgent scientific and industrial needs. The importance of electrospun fibres is constantly increasing, while electrospinning

can be considered as a complementary technology to others, especially spray drying. ASDs with advantageous characteristics can be produced by electrospinning but compared to spray drying or melt extrusion, downstream processing and tablet formulation are not elaborated. Dynamic vapour sorption measurement was carried out to assess behaviour of EM under high and increasing humidity and two different temperatures (25 and 40 °C). At 25 °C phases got separated, however, only higher temperature (40 °C) induced slow recrystallization. Based on the DVS isotherms, "glass transition humidity" was calculated (72%) and possible storage conditions were deducted (25 °C/60% RH, open conditions).

The tablet composition and compression force were optimized by applying an experimental design with dependent variables of disintegration time and tensile strength. It was found that EM is prone to cover excipient particles with structured surface such as microcrystalline cellulose or lactose (but not mannitol) and occupies a significant volume in blends and tablets. These can influence the flowability of the tableting blend, the dissolution properties (e.g. wetting) and the formation of a gelling polymer network. This might apply to spray dried ASDs as well due to their small particle size and low bulk density. Fibrous structure of EM could be preserved during the whole downstream processing. Scanning electron microscope images confirmed the presence of fibres even in tablets. The results demonstrate the feasibility of converting a nanofibrous electrospun mat to industrially applicable tablets.

References

[1] W.L. Chiou, S. Riegelman, Pharmaceutical applications of solid dispersion systems, J. Pharm. Sci. 60 (1971) 1281–1302.

[2] C.L.-N. Vo, C. Park, B.-J. Lee, Current trends and future perspectives of solid dispersions containing poorly water-soluble drugs, Eur. J. Pharm. Biopharm. 85 (2013) 799–813.

[3] A. Serajuddin, Solid dispersion of poorly water-soluble drugs: early promises, subsequent problems, and recent breakthroughs, J. Pharm. Sci. 88 (1999) 1058–1066.

[4] A. Paudel, Z.A. Worku, J. Meeus, S. Guns, G. Van den Mooter, Manufacturing of solid dispersions of poorly water soluble drugs by spray drying: formulation and process considerations, Int. J. Pharm. 453 (2013) 253–284.

[5] S. Page, R. Maurer, Downstream processing considerations, in: N. Shah, H. Sandhu, S.D. Choi, H. Chokshi, W.A. Malick (Eds.), Amorphous Solid Dispersions: Theory and Practice, Springer, New York, New York, NY, 2014, pp. 395–417.

[6] A. Singh, G. Van den Mooter, Spray drying formulation of amorphous solid dispersions, Adv. Drug Deliv. Rev. 100 (2016) 27–50.

[7] H. Patil, R.V. Tiwari, M.A. Repka, Hot-melt extrusion: from theory to application in pharmaceutical formulation, AAPS Pharm. Sci. Technol. 17 (2016) 20–42.

[8] P. Kanaujia, P. Poovizhi, W.K. Ng, R.B.H. Tan, Amorphous formulations for dissolution and bioavailability enhancement of poorly soluble APIs, Powder Technol. 285 (2015) 2–15.

[9] B. Démuth, Z. Nagy, A. Balogh, T. Vigh, G. Marosi, G. Verreck, I. Van Assche, M. Brewster, Downstream processing of polymer-based amorphous solid dispersions to generate tablet formulations, Int. J. Pharm. 486 (2015) 268–286.

[10] G. Verreck, K. Heymans, D. Henrist, I. Van Assche, L. Baert, G. Van den Mooter, M.E. Brewster, Post-die processing of solid dispersion-based melt extrudates: milling and tableting, in: AAPS Annual Meeting and Exposition, 2013.

[11] F. Jijun, Z. Lili, G. Tingting, T. Xing, H. Haibing, Stable nimodipine tablets with high bioavailability containing NM-SD prepared by hot-melt extrusion, Powder Technol. 204 (2010) 214–221.

[12] L. Baert, C. Elvire, G. Verreck, Antiretroviral compositions with improved bioavailability, Eur. Pat. 872 (1997) 233.

[13] S. Sharif, L.M. DiMemmo, M. Thommes, M. Hubert, B.A. Sarsfield, A simplified approach to determine effective surface area and porosity of low bulk density active pharmaceutical ingredients in early development, Adv. Powder Technol. 26 (2015) 337–348.

[14] H. Yue, S.J. Nicholson, J.D. Young, D. Hsieh, R.J. Ketner, R.G. Hall, J. Sackett, E.C. Banks, J.A. Castoro, M.E. Randazzo, Development of a control strategy for benzene impurity in HPMCAS-stabilized spray-dried dispersion drug products using a science-based and risk-based approach, Pharm. Res. (2015) 1–13.

[15] S. Reven, M. Homar, L. Peternel, J. Kristl, E. Žagar, Preparation and characterization of tablet formulation based on solid dispersion of glimepiride and poly(ester amide) hyperbranched polymer, Pharm. Dev. Technol. 18 (2013) 323–332.

[16] M.M. Leane, W. Sinclair, F. Qian, R. Haddadin, A. Brown, M. Tobyn, A.B. Dennis, Formulation and process design for a solid dosage form containing a spray-dried amorphous dispersion of ibipinabant, Pharm. Dev. Technol. 18 (2013) 359–366.

[17] F. Jijun, X. Lishuang, W. Xiaoli, Z. Shu, T. Xiaoguang, Z. Xingna, H. Haibing, T. Xing, Nimodipine (NM) tablets with high dissolution containing NM solid dispersions prepared by hot-melt extrusion, Drug Dev. Ind. Pharm. 37 (2011) 934–944.

[18] Z. Ayenew, A. Paudel, G. Van den Mooter, Can compression induce demixing in amorphous solid dispersions? A case study of naproxen–PVP K25, Eur. J. Pharm. Biopharm. 81 (2012) 207–213.

[19] A.B. Joshi, S. Patel, A.M. Kaushal, A.K. Bansal, Compaction studies of alternate solid forms of celecoxib, Adv. Powder Technol. 21 (2010) 452–460.

[20] D.-G. Yu, X.-Y. Li, X. Wang, J.-H. Yang, S.A. Bligh, G.R. Williams, Nanofibers fabricated using triaxial electrospinning as zero order drug delivery systems, ACS Appl. Mater. Interfaces. 7 (2015) 18891–18897.

[21] D.-G. Yu, G.R. Williams, X. Wang, X.-K. Liu, H.-L. Li, S.A. Bligh, Dual drug release nanocomposites prepared using a combination of electrospraying and electrospinning, RSC Adv. 3 (2013) 4652–4658.

[22] B. Démuth, A. Farkas, H. Pataki, A. Balogh, B. Szabó, E. Borbás, P.L. Sóti, T. Vigh, É. Kiserdei, B. Farkas, J. Mensch, G. Verreck, I. Van Assche, G. Marosi, Z.K. Nagy, Detailed stability investigation of amorphous solid dispersions prepared by single-needle and high speed electrospinning, Int. J. Pharm. 498 (2016) 234–244.

[23] E. Borbás, A. Balogh, K. Bocz, J. Müller, É. Kiserdei, T. Vigh, B. Sinkó, A. Marosi, A. Halász, Z. Dohányos, L. Szente, G.T. Balogh, Z.K. Nagy, In vitro dissolution–permeation evaluation of an electrospun cyclodextrin-based formulation of aripiprazole using μFlux™, Int. J. Pharm. 491 (2015) 180–189.

[24] Z.K. Nagy, A. Balogh, B. Vajna, A. Farkas, G. Patyi, Á. Kramarics, G. Marosi, Comparison of electrospun and extruded soluplus®-based solid dosage forms of improved dissolution, J. Pharm. Sci. 101 (2012) 322–332.

[25] X. Wang, X.-Y. Li, Y. Li, H. Zou, D.G. Yu, J.-S. Cai, Electrospun acetaminophen-loaded cellulose acetate nanofibers fabricated using an epoxy-coated spinneret, e-Polymers 15 (2015) 311–315.

[26] Z.K. Nagy, A. Balogh, B. Demuth, H. Pataki, T. Vigh, B. Szabo, K. Molnar, B.T. Schmidt, P. Horak, G. Marosi, G. Verreck, I. Van Assche, M.E. Brewster, High speed electrospinning for scaled-up production of amorphous solid dispersion of itraconazole, Int. J. Pharm. 480 (2015) 137–142.

[27] U.E. Illangakoon, H. Gill, G.C. Shearman, M. Parhizkar, S. Mahalingam, N.P. Chatterton, G.R. Williams, Fast dissolving paracetamol/caffeine nanofibers prepared by electrospinning, Int. J. Pharm. 477 (2014) 369–379.

[28] F.L. Lopez, G.C. Shearman, S. Gaisford, G.R. Williams, Amorphous formulations of indomethacin and griseofulvin prepared by electrospinning, Mol. Pharm. 11 (2014) 4327–4338.

[29] J. Pelipenko, P. Kocbek, J. Kristl, Critical attributes of nanofibers: preparation, drug loading, and tissue regeneration, Int. J. Pharm. 484 (2015) 57–74.

[30] H.-W. Kim, H.-H. Lee, J.C. Knowles, Electrospinning biomedical nanocomposite fibers of hydroxyapatite/poly(lactic acid) for bone regeneration, J. Biomed. Mater. Res., Part A 79A (2006) 643–649.

[31] W.-J. Li, C.T. Laurencin, E.J. Caterson, R.S. Tuan, F.K. Ko, Electrospun nanofibrous structure: a novel scaffold for tissue engineering, J. Biomed. Mater. Res. 60 (2002) 613–621.

[32] S. Petrik, M. Maly, Production nozzle-less electrospinning nanofiber technology, MRS Proc. 1240 (2009) (1240-WW1203-1207).

[33] K. Molnár, B. Szolnoki, A. Toldy, L.M. Vas, Thermochemical stabilization and analysis of continuously electrospun nanofibers, J. Therm. Anal. Calorim. 117 (2014) 1123–1135.

[34] G. Verreck, I. Chun, J. Peeters, J. Rosenblatt, M.E. Brewster, Preparation and characterization of nanofibers containing amorphous drug dispersions generated by electrostatic spinning, Pharm. Res. 20 (2003) 810–817.

[35] G. Verreck, I. Chun, J. Rosenblatt, J. Peeters, A. Van Dijck, J. Mensch, M. Noppe, M.E. Brewster, Incorporation of drugs in an amorphous state into electrospun nanofibers composed of a water-insoluble, nonbiodegradable polymer, J. Control. Release 92 (2003) 349–360.

[36] R.K. Deshmukh, J.B. Naik, The impact of preparation parameters on sustained release aceclofenac microspheres: a design of experiments, Adv. Powder Technol. 26 (2015) 244–252.

[37] J. Fell, J. Newton, Determination of tablet strength by the diametral-compression test, J. Pharm. Sci. 59 (1970) 688–691.

[38] D.J. Burnett, F. Thielmann, J. Booth, Determining the critical relative humidity for moisture-induced phase transitions, Int. J. Pharm. 287 (2004) 123–133.

[39] K. Six, G. Verreck, J. Peeters, P. Augustijns, R. Kinget, G. Van den Mooter, Characterization of glassy itraconazole: a comparative study of its molecular mobility below Tg with that of structural analogues using MTDSC, Int. J. Pharm. 213 (2001) 163–173.

[40] M. Vasanthavada, W.-Q.T. Tong, Y. Joshi, M.S. Kislalioglu, Phase behavior of amorphous molecular dispersions II: role of hydrogen bonding in solid solubility and phase separation kinetics, Pharm. Res. 22 (2005) 440–448.

[41] M. Tarnacka, K. Adrjanowicz, E. Kaminska, K. Kaminski, K. Grzybowska, K. Kolodziejczyk, P. Wlodarczyk, L. Hawelek, G. Garbacz, A. Kocot, Molecular dynamics of itraconazole at ambient and high pressure, Phys. Chem. Chem. Phys. 15 (2013) 20742–20752.

[42] J.M. Juran, Juran on Quality by Design the New Steps for Planning Quality Into Goods and Services, Simon and Schuster, 1992.

[43] L.X. Yu, Pharmaceutical quality by design: product and process development, understanding, and control, Pharm. Res. 25 (2008) 781–791.

[44] P. Kaur, S.K. Singh, V. Garg, M. Gulati, Y. Vaidya, Optimization of spray drying process for formulation of solid dispersion containing polypeptide-k powder through quality by design approach, Powder Technol. 284 (2015) 1–11.